

Mechanisms of very fast oscillations in networks of axons coupled by gap junctions

Erin Munro · Christoph Börgers

Received: 30 July 2009 / Revised: 4 March 2010 / Accepted: 17 March 2010
© Springer Science+Business Media, LLC 2010

Abstract Because electrical coupling among the neurons of the brain is much faster than chemical synaptic coupling, it is natural to hypothesize that gap junctions may play a crucial role in mechanisms underlying very fast oscillations (VFOs), i.e., oscillations at more than 80 Hz. There is now a substantial body of experimental and modeling literature supporting this hypothesis. A series of modeling papers, starting with work by Roger Traub and collaborators, have suggested that VFOs may arise from expanding waves propagating through an “axonal plexus”, a large random network of electrically coupled axons. Traub et al. also proposed a cellular automaton (CA) model to study the mechanisms of VFOs in the axonal plexus. In this model, the expanding waves take the appearance of topologically circular “target patterns”. Random external stimuli initiate each wave. We therefore call this kind of VFO “externally driven”. Using a computational model, we show that an axonal plexus can also exhibit a second, distinctly different kind of VFO in a wide parameter range. These VFOs arise from activity propagating around cycles in the network. Once triggered, they persist without any source of excitation. With idealized, regular connectivity, they take the appearance of spiral

waves. We call these VFOs “re-entrant”. The behavior of the axonal plexus depends on the reliability with which action potentials propagate from one axon to the next, which, in turn, depends on the somatic membrane potential V_s and the gap junction conductance g_{gj} . To study these dependencies, we impose a fixed value of V_s , then study the effects of varying V_s and g_{gj} . Not surprisingly, propagation becomes more reliable with rising V_s and g_{gj} . Externally driven VFOs occur when V_s and g_{gj} are so high that propagation never fails. For lower V_s or g_{gj} , propagation is nearly reliable, but fails in rare circumstances. Surprisingly, the parameter regime where this occurs is fairly large. Even a single propagation failure can trigger re-entrant VFOs in this regime. Lowering V_s and g_{gj} further, one finds a third parameter regime in which propagation is unreliable, and no VFOs arise. We analyze these three parameter regimes by means of computations using model networks adapted from Traub et al., as well as much smaller model networks.

Keywords Axonal plexus · Axon · Gap junction · Very fast oscillation · Ripple · Epilepsy

1 Introduction

Very fast oscillations (VFOs) in the brain, i.e., oscillations at frequencies greater than 80 Hz, have been associated with resting and sleep as well as epilepsy and seizure initiation (Bragin et al. 1999, 2002, 2004; Clemens et al. 2007; Fisher et al. 1992; Grenier et al. 2001, 2003; Jacobs et al. 2008; Maier et al. 2003; Roopun et al. 2010; Staba et al. 2004; Traub et al. 2001, 2005, 2009; Traub 2003; Urrestarazu et al. 2007;

Action Editor: Charles Wilson

E. Munro (✉)
Department of Mathematics and Center for Biodynamics,
Boston University, Boston, MA 02215, USA
e-mail: ecmun@bu.edu

C. Börgers
Department of Mathematics, Tufts University, Medford,
MA 02155, USA

Worrell et al. 2004; Ylinen et al. 1995). A substantial body of experimental and modeling literature suggests that gap junctions may be important in mechanisms underlying VFOs (Draguhn et al. 1998; Grenier et al. 2001, 2003; Lewis and Rinzel 2000, 2001; Maex and De Schutter 2007; Middleton et al. 2008; Roopun et al. 2010; Schmitz et al. 2001; Traub et al. 1999, 2001, 2003a, 2008, 2009; Traub and Bibbig 2000; Traub 2003; Tseng et al. 2008). In the present work, we focus on a series of modeling papers, starting with Traub et al. (1999). Traub et al. suggest that VFOs may reflect waves of activity propagating through an “axonal plexus”, i.e., a network of gap-junctionally coupled axons. Draguhn et al. (1998) first hypothesized the existence of axo-axonal gap junctions in order to explain the presence of spikelets (miniature action potentials ranging in amplitude from 3–15 mV) in pyramidal cell somata. Unlike typical gap junctions connecting dendrites, gap junctions between axons can allow action potentials to propagate from one axon to another and hence travel antidromically to the soma as well as to other axons. There is indirect experimental and modeling evidence for the existence of networks of electrically coupled pyramidal cell axons in hippocampus (Draguhn et al. 1998; Schmitz et al. 2001), cortex (Grenier et al. 2001, 2003; Roopun et al. 2010), and cerebellum (Middleton et al. 2008). Hamzei-Sichani et al. (2007) have presented direct evidence for gap-junctional coupling between pairs of mossy fiber axons in rat hippocampus.

In the model of Traub et al. (1999), the waves are fueled by somatic firing and Poisson trains of excitatory inputs. In Traub et al. (1999, Appendix) also proposed a cellular automaton (CA) model, a stochastic version of the Greenberg–Hastings model (Greenberg and Hastings 1978), to understand the mechanisms underlying VFOs. This model was analyzed in detail by Lewis and Rinzel (2000), who found that the VFOs are based on expanding waves. The waves are “topologically closed”, in the sense that the only way to cross from one side of a wave to the other via the network is to pass through the wave. When two or more such waves collide, they merge and form a larger topologically closed wave. The waves continue to expand, collide and merge in this manner until they reach the edge of the network. Each wave must be initiated by an external stimulus. Thus, we call VFOs based on this mechanism “externally driven”.

The mechanism of externally driven VFOs requires reliable propagation of action potentials through gap junctions. As pointed out in Lewis and Rinzel (2000), propagation failures lead to uni-directional waves, which in turn can result in self-sustaining periodic “re-entrant” waves. In our model, the reliability of propa-

gation depends on the membrane potentials V_s of the somata to which the axons are attached, and on the gap junction conductance g_{gj} . Propagation is reliable if the somata are sufficiently depolarized or gap-junctional coupling among axons is sufficiently strong. We find a large domain of intermediate values of V_s or g_{gj} for which propagation is *nearly reliable*, but fails in rare circumstances. In this parameter range, one typically sees re-entrant activity. Re-entrant activity takes on the appearance of spiral waves if the connectivity is sufficiently regular. Thus this type of activity in the plexus resembles the spiral waves in cardiac tissue seen in fibrillation; see Veenhuyzen et al. (2004) for a recent review.

When V_s and g_{gj} are low, propagation of action potentials fails frequently. As a result, the VFOs are abolished, and the plexus simply responds to noisy excitatory drive with non-oscillatory, noisy activity.

We thus distinguish three types of network activity: externally driven VFOs, re-entrant activity, and noise. By means of numerical computations, we show that axons connected to the largest number of neighbors play a key role in determining which of these three behaviors is seen. In the model of Traub et al. (1999), the maximum number of electrically coupled neighbors is 4. The axons that are coupled to four neighbors, which we will refer to as “four-connected axons”, are most strongly shunted by their neighbors, and therefore most likely to block propagation.

For high V_s or g_{gj} , four-connected axons always propagate action potentials. However, as V_s or g_{gj} is lowered, signal propagation begins to become somewhat unreliable. The four-connected axons are still capable of propagating a single signal, but the hyperpolarization of their neighbors in the wake of a signal prevents them from spiking a second time in rapid succession. Because the effective refractory period of an axon is determined by the hyperpolarization of its neighbors, four-connected axons have a longer effective refractory period than axons with fewer connections. When two signals reach a four-connected cell in rapid succession, the second is blocked. We note that what matters here is not the absolute length of the refractory period, but rather the differences in refractory periods between different axons. If all axons had refractory periods of the same length, a second signal would never reach a four-connected cell too soon after the first, and therefore no signal would be blocked. It is the *heterogeneity* in effective refractory periods which enables propagation block, with a resulting re-entrant wave.

For low values of V_s or g_{gj} , signal propagation is almost always blocked by four-connected axons. This

effectively removes the four-connected axons from the network, breaking the network into many much smaller disconnected components. Local averages of activity are then non-periodic and noisy.

2 Methods

Axon model We use the five axonal compartments of the model of Traub et al. (1999) in our study (see Fig. 1). The membrane potential, V_k , of the k -th compartment is modeled by a Hodgkin–Huxley type equation:

$$C_k \frac{dV_k}{dt} = -g_{L,k}V_k + \bar{g}_{Na,k}m_k^3h_k(V_{Na} - V_k) + \bar{g}_{K,k}n_k^4(V_K - V_k) + \sum_l \gamma_{l,k}(V_l - V_k) + I_{\text{ext},k} \quad (1)$$

The index l in the sum runs over all compartments adjacent to the k -th compartment, and

C_k	= capacitance,
$g_{L,k}$	= leak conductance,
$\bar{g}_{Na,k}$	= sodium conductance,
$\bar{g}_{K,k}$	= delayed rectifier potassium conductance,
V_{Na}	= sodium reversal potential = 115 mV,

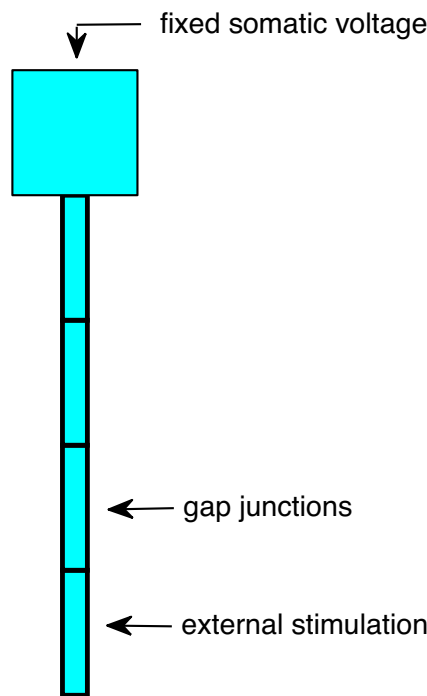


Fig. 1 Model axon

V_K	= potassium reversal potential = −15 mV,
m_k, h_k, n_k	= sodium and potassium gating variables,
$\gamma_{l,k} = \gamma_{k,l}$	= conductance between compartments k and l ,
$I_{\text{ext},k}$	= external current.

The gating variables m_k , h_k , and n_k are governed by equations of the form

$$\frac{dz_k}{dt} = \alpha_z(V_k)(1 - z_k) - \beta_z(V_k)z_k, \quad z = m, h, n.$$

The functions, α_z and β_z , for each gating variable are given in Table 1.

The definitions of the capacitances and conductances are motivated as follows. Each compartment is modeled as a cylinder. The radius of the initial segment is $r_1 = 2 \mu\text{m}$, and the radius of all other axonal compartments ($k = 2, 3, 4, 5$) is $r_k = 0.5 \mu\text{m}$. The length of each compartment is $L = 75 \mu\text{m}$. For all compartments, the capacitance density is $C_m = 0.75 \mu\text{F}/\text{cm}^2$, the leak conductance density is $g_L = 1 \text{ mS}/\text{cm}^2$, the sodium conductance density is $\bar{g}_{Na} = 500 \text{ mS}/\text{cm}^2$, and the potassium conductance density is $\bar{g}_K = 250 \text{ mS}/\text{cm}^2$. The total capacitance and conductances for compartment k are obtained by multiplying these densities by the surface area $2\pi r_k L$ of the k -th compartment.

The conductance between compartments $\gamma_{l,k}$ is determined by the equation

$$\frac{1}{\gamma_{l,k}} = \frac{1}{2} \frac{R_i L}{\pi r_k^2} + \frac{1}{2} \frac{R_i L}{\pi r_l^2}, \quad (2)$$

where R_i is the internal resistivity, taken to be $100 \Omega\text{cm}$. The two summands on the right-hand side of Eq. (2) are the internal resistances of one half of compartment k , and one half of compartment l . (This makes sense if one thinks of V_k and V_l as the voltages in the centers of the cylindrical compartment.)

In the simulations of Traub et al. (1999), the somatic membrane potentials V_s vary on a time scale that is long in comparison with the period of the VFOs in the axonal plexus. We therefore make the simplifying assumption that the initial segment is electrically cou-

Table 1 Gating variable functions $\alpha_z(V)$ and $\beta_z(V)$ for $z = m, h, n$

Gating variable	$\alpha_z(V)$	$\beta_z(V)$
m	$\frac{0.8(17.2 - V)}{\exp((17.2 - V)/4) - 1}$	$\frac{0.7(V - 42.2)}{\exp((V - 42.2)/5) - 1}$
h	$0.32 \exp((42 - V)/18)$	$\frac{10}{1 + \exp((42 - V)/5)}$
n	$\frac{0.03(17.2 - V)}{\exp((17.2 - V)/5) - 1}$	$0.45 \exp((12 - V)/40)$

pled to a soma held at a fixed, constant membrane potential V_s :

$$I_{\text{ext},1} = \gamma_{s,1}(V_s - V_1).$$

The conductance $\gamma_{s,1}$ is defined by a formula analogous to Eq. (2):

$$\frac{1}{\gamma_{s,1}} = \frac{1}{2} \frac{R_{i,s} L_s}{\pi r_s^2} + \frac{1}{2} \frac{R_i L}{\pi r_1^2},$$

where $r_s = 15 \mu\text{m}$ denotes the radius of the soma (which is also modeled as a cylinder), $L_s = 25.5 \mu\text{m}$ is its length, and $R_{i,s} = 200 \Omega\text{cm}$ is the internal resistivity of the soma (Traub et al. 1999). Thus the soma is not modeled explicitly in our paper; its only role is to provide a boundary condition. We use values of V_s in the range seen in Traub et al. (1999) (where the somatic voltage is modeled, not imposed). Lewis and Rinzel (2001) used the same five-compartment axonal model, but with a different boundary condition: the initial segment had a sealed end in their model.

Large network model We adopt the model network of Traub et al. (1999), but alter it in two ways: First, we remove the somatic and dendritic compartments as described above. Second, we experiment with different values of the gap junction conductance g_{gj} , varying g_{gj} to reproduce the different types of network behavior seen in Traub et al. (1999, 2000, 2003a, b), Traub and Bibbig (2000).

We briefly summarize important features of the network in Traub et al. (1999). There are 3,072 axons altogether. They are placed on a 32×96 rectangular grid, with unit grid spacing in both coordinate directions. The random network connectivity is determined as follows. An axon A is chosen at random, with each axon equally likely. Then a second axon B is chosen at random from a 21×21 grid centered at A . Note that the 21×21 grid may extend beyond the boundary of the large 32×96 grid if A lies close to the edge. Axons A and B are connected if (1) B belongs to the original grid, (2) the euclidean distance between A and B is ≤ 10 , and (3) neither of the two axons are coupled to four neighbors yet. This procedure is then repeated until the total number of connections reaches 2,458 ($0.8 \times 3,072$, rounded to the nearest integer). Thus the average number of neighbors to which a given axon is connected is $2 \times 0.8 = 1.6$, and the maximum number is 4.

This network can be viewed as a random graph. It is different from the random graphs in the classical paper by Erdős and Rényi (1960). The most important difference perhaps is that in our network, connections are constrained to be local. Nonetheless, numerical results in Traub et al. (1999) suggest that the theory

of Erdős and Rényi does describe the structure of our network well. The mean number of neighbors per node, 1.6, is well above the threshold found by Erdős and Rényi, which is 1.0. Thus one expects that there is one very large connected cluster in the graph; numerical experiments confirm this (Traub et al. 1999).

Gap junctions are located on the fourth (second-most distal) axonal compartment. Therefore in Eq. (1), the external membrane current for compartment 4 of axon i is

$$I_{\text{ext},4,i} = \sum_j g_{gj}(V_{4,j} - V_{4,i}),$$

where j runs over all axons that are gap-junctionally coupled to axon i . Random excitatory stimuli (0.2 nA currents applied for 0.3125 ms) arrive on a Poisson schedule at a rate of 2/s/axon, at the fifth (most distal) compartment.

Small network models In addition to the large network model, we also simulate much smaller networks to explore in detail how local connectivity affects signal propagation. We quantify the connectivity-dependent heterogeneity in refractory periods that can lead to propagation failures when two waves arrive in quick succession.

Our small networks are shown in Fig. 2. We primarily focus on axon 2. The networks are labeled “ m - n ”, where m is the number of neighbors to which axon 2 is coupled, and n is the number of neighbors to which axon 3 is coupled. We will define a quantity t_f that can be interpreted as the difference in refractory periods between axons 1 and 2.

We stimulate axon 1 (as in the large network model, i.e., as in Traub et al. (1999)) twice in succession, varying the time interval between stimulations, and record the resulting spiking activity. We say that an axon “spikes” when the membrane potential of the second-most-distal compartment crosses 50 mV from below. The simulation is started at $t = 0$ ms. The first stimulation of axon 1 arrives at $t = 10$ ms, and always promptly triggers a spike of axon 1. After this spike, axon 1 becomes refractory; if the second stimulation arrives too soon, axon 1 does not spike again. We denote the earliest time at which axon 1 can spike again, in response to the second stimulation, by t_1 ; see the upper panel of Fig. 3.

Whether or not axon 2 can fire at all in response to a spike of axon 1 depends on the strength of the gap-junctional coupling and the somatic voltage. If axon 2 fires after axon 1 fires, then it can eventually fire again in response to axon 1, provided axon 1 does not fire earlier than some time $t_2 \geq t_1$; see the lower panel of Fig. 3. We call the time interval from t_1 to t_2 the “time

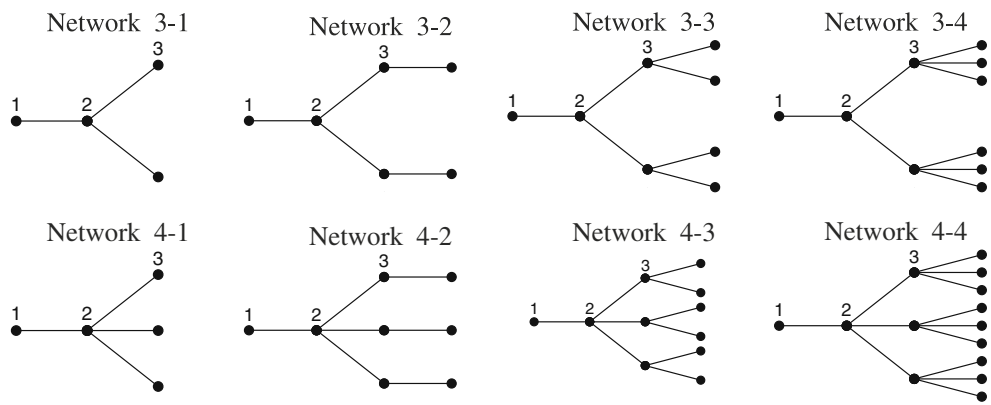


Fig. 2 Small networks used to determine how local connectivity affects propagation failure. The nodes represent axons, while the connections represent gap junctions. In small network simulations, axon 1 is stimulated and so activity flows from *left to right* in each network. Networks are numbered $m-n$ according to their

connections, where m is the number of neighbors for axon 2, and n is the number of neighbors for axon 3. In general, there is less shunting in axon 2 when there are fewer downstream neighbors. These networks represent the range of “gap-junctional loads” that three-connected and four-connected axons can experience

interval of propagation failure”. We denote the length of this interval by t_f , so $t_f = t_2 - t_1$. If spikes of axon 1 never trigger spikes of axon 2, we set $t_f = \infty$.

Cellular automata In the CA model of (Traub et al. 1999, Appendix), each cell (axon) has three possible states: resting, excited (or “on”), and refractory. The

life cycle of the CA is as follows. Cells are “resting” until they are turned “on”. After they are “on” for one time step, they are “refractory” for t_r time steps, then return to the “resting” state. Diagrammatically, the life cycle of a cell is:

$$\text{resting} \rightarrow \text{excited} \rightarrow \text{refractory} \rightarrow \dots \\ \rightarrow \text{refractory} \rightarrow \text{resting}$$

Cells turn on either when they are stimulated externally or when one of their neighbors is on for the previous time step. Cells are stimulated randomly according to independent Poisson processes. As in Lewis and Rinzel (2000), we take one time step to be equivalent to 0.25 ms. Since typical refractory periods in the axonal plexus model are slightly below 3 ms when there is re-entrant activity, we use $t_r = 11$. (Lewis and Rinzel (2000) used $t_r = 3$.)

We also experiment with two modifications of this CA. In the first modification, four-connected cells are turned on only when two of their immediate neighbors are turned on, or when they are directly stimulated. In the second modification, four-connected cells have a longer refractory period than other cells: $t_r \geq 12$ (we experiment with different values).

Computational aspects Our codes for simulating the large and small network models are written in C, and can be accessed in ModelDB.¹ Our code reproducing (Traub et al. 1999, Figure 12) (see our Fig. 12) uses MPI for parallel processing. Following Traub et al. (1999), we always use the midpoint method for numerical integration with a time step of 0.0025 ms. We

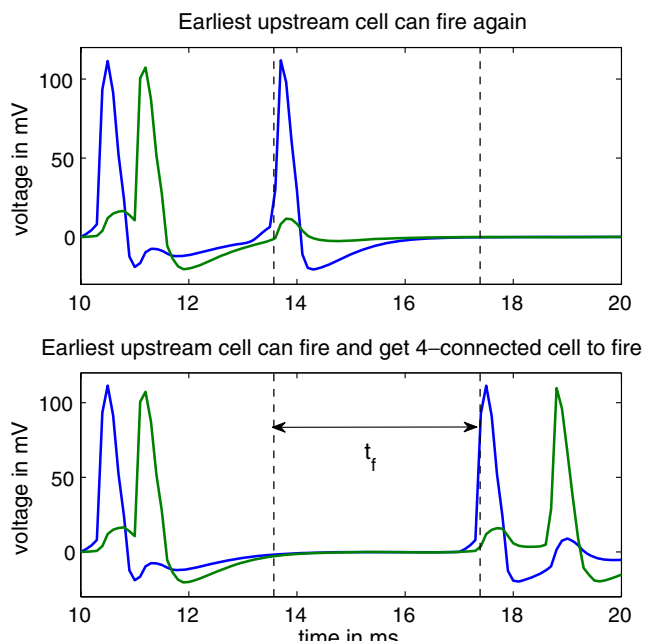


Fig. 3 Definition of the interval of propagation failure for an axon A relative to an upstream neighbor B . (The length of the interval is t_f .) The figure shows results where A is axon 2 in network 4-1 with $V_s = 0$ mV and $g_{gj} = 3.8$ nS. The voltage trace of A is shown in green while the voltage trace of B (axon 1 in network 4-1) is shown in blue. The interval of propagation failure is delineated by the dashed black lines. See text for details

¹<http://senselab.med.yale.edu/modeldb/>, accession number 120907.

use MATLAB for cellular automata and data analysis. The computations for this paper were performed on the Tufts Linux Research Cluster. A simulation of the large network over a 100 ms time window took approximately 30 min on one processor of those machines. The reproduction of (Traub et al. 1999, Figure 12) took approximately 48 h on 16 processors.

3 Results

3.1 Observed network behavior

We simulated a model network of axons connected by gap junctions based on Traub et al. (1999), as described in Section 2. Our model differs from that of Traub et al. (1999) in that we remove the somata and dendrites, and apply instead a fixed somatic voltage to the axon initial segment; see Fig. 1. The network showed three different types of behavior, depending on the gap junction conductance, g_{gj} , and the fixed somatic voltage, V_s : externally driven very fast oscillations (VFOs), re-entrant activity, and non-oscillatory noisy activity.

Externally driven VFOs An example of externally driven VFOs is shown in Fig. 4; here $g_{gj} = 6 \text{ nS}$ and

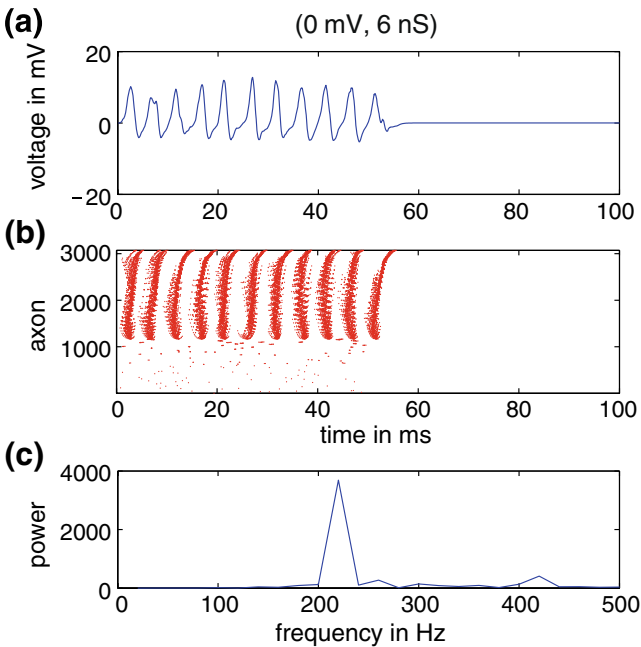


Fig. 4 Externally driven VFOs. Average voltage of second-most-distal compartments (a), rastergram (b), and power spectrum (c). The axons in the rastergram are arranged by cluster. The smaller clusters are at the *bottom*, and the large cluster at the *top*. Waves propagate throughout the large cluster. Activity stops shortly after stimulation stops at $t = 50 \text{ ms}$

$V_s = 0 \text{ mV}$. As noted in Traub et al. (1999), there is a large connected cluster in the network, comprising most of the network, and there are many much smaller clusters. As described in Lewis and Rinzel (2000, 2001), after an axon is stimulated, an expanding wave forms around that axon and propagates through the network. All activity stops soon after external stimulation stops at $t = 50 \text{ ms}$. Because each expanding wave is initiated in a different axon, the individual waves do not look identical to each other, although they are qualitatively similar.

Re-entrant activity Reducing the gap junction conductance to $g_{gj} = 4.5 \text{ nS}$, we obtain re-entrant activity; see Fig. 5. As in the previous simulation, activity propagates in waves through the large cluster, but continues after stimulation ceases. As discussed in Lewis and Rinzel (2000), this kind of re-entrant activity can arise when there is a propagation failure, breaking the symmetry of an expanding wave. In Fig. 5, this probably happens at $t = 10$, long before the stimulation ceases, since this is when different waves begin looking very similar to each other. Notice that after the stimulation ceases, all waves look perfectly identical to each other. This reflects the fact that all network activity is generated from a wave continually propagating around a cycle in the network.

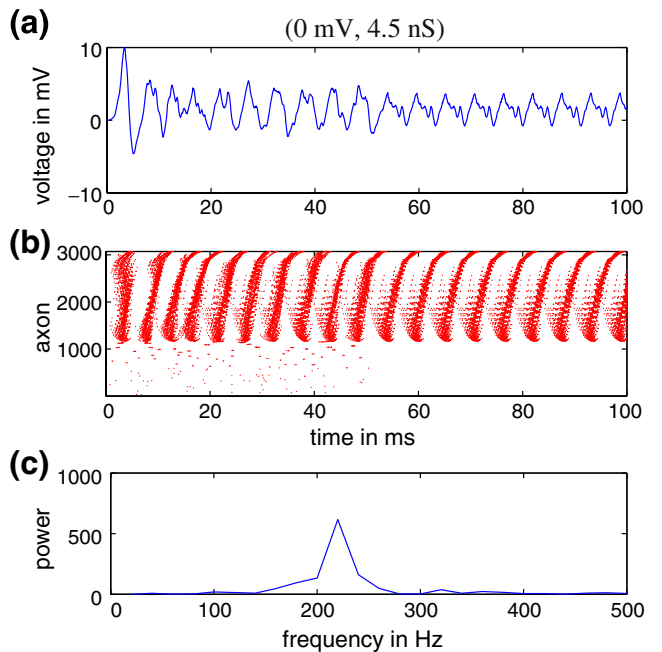


Fig. 5 Re-entrant VFOs. Average voltage of second-most-distal compartments (a), rastergram (b), and power spectrum (c) for $V_s = 0 \text{ mV}$ and $g_{gj} = 4.5 \text{ nS}$. Activity continues after stimulation ceases at $t = 50 \text{ ms}$

Non-oscillatory noisy activity Reducing the gap junction conductance further to 3.7 nS, we obtain non-oscillatory noisy activity; see Fig. 6. There are now many propagation failures, and as a result waves only partially propagate within the large cluster. Since the partial waves occur independently of each other, the average voltage appears noisy. When stimulation ceases, all activity dies down immediately.

3.2 Parameter regimes

Fixing the random network connectivity, we varied V_s and g_{gj} . For each pair (V_s, g_{gj}) , we performed 10 simulations with different random number generator seeds, each time simulating 100 ms. We applied random excitatory stimuli during the first half of each simulation (the first 50 ms), and removed the stimuli during the second half.

We ran simulations for parameter pairs (V_s, g_{gj}) with $-3 \leq V_s \leq 3$, and $2.5 \leq g_{gj} \leq 6$. The somatic voltage range was chosen to reflect the values of sub-threshold somatic voltages observed in the full CA3 pyramidal cell model Traub et al. (1999). The range of gap junction conductances was chosen to reproduce the various

behaviors seen in Traub et al. (1999, 2000, 2003a, b), Traub and Bibbig (2000).

For each individual simulation, we classified the observed activity as follows. If there was any spiking in the last 5 ms of the simulation, we classified the activity as “re-entrant”. If the activity was not classified as “re-entrant”, we analyzed the discrete time series of the first 50 ms of the average voltage of the second-most-distal compartments,

$$v_j = v(j/10), \quad 0 \leq j \leq 500$$

by calculating the power spectrum (see Appendix). We denote the maximum power over all nonzero frequencies by P . In all cases for which we have looked at voltage traces, pronounced oscillations correspond to large P , while noise corresponds to small P (see also Appendix). We therefore classified the activity as an “externally driven VFO” if

$$P \geq 50 \quad (3)$$

and as “noise” if $P < 50$. We empirically observed that a value of $P \geq 50$ indicates that a substantial number of axons are firing synchronously. Almost always, the activity either had the clear appearance of oscillations with $P \gg 50$, or the clear appearance of noise with $P \ll 50$.

For low V_s and g_{gj} , all 10 simulations exhibited noise. For high V_s and g_{gj} , all 10 simulations exhibited externally driven VFOs. For a wide range of intermediate parameter pairs (V_s, g_{gj}) , some simulations exhibited re-entrant activity while others exhibited externally driven VFOs. There were a few parameter pairs (V_s, g_{gj}) where some simulations showed re-entrant activity while others showed noise. There were no parameters for which some simulations showed externally driven VFOs and others showed noise.

The results are shown in Fig. 7. The black boundaries outline the region where re-entrant activity occurs with $\geq 50\%$ probability. We refer to this region as the re-entrant activity regime. The noise regime lies below the re-entrant activity regime, and the externally driven VFO regime lies above.

For each simulation labeled re-entrant activity or externally driven VFOs, we determined the frequency with the maximum power. For externally driven VFOs, the mean frequency was 208 Hz, with a standard deviation of 13 Hz. For re-entrant VFOs, the mean frequency was 250 Hz, and the standard deviation 80 Hz.² The

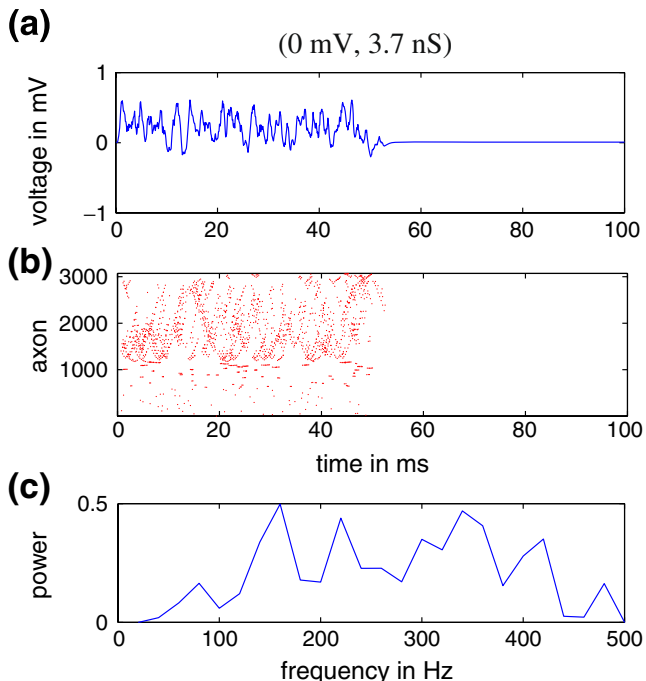
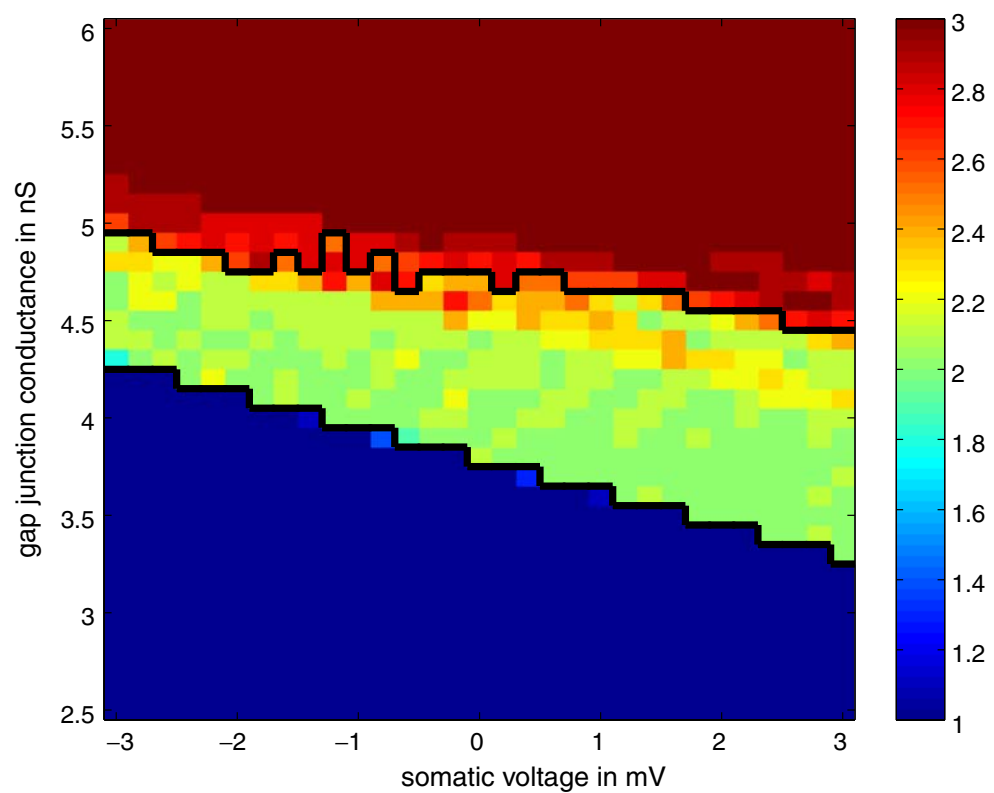


Fig. 6 Noise. Average voltage of second-most-distal compartments (a), rastergram (b), and power spectrum (c) for $V_s = 0$ mV and $g_{gj} = 3.7$ nS. Note that the scaling of the vertical axis in the bottom panel is very different here than in Figs. 4 and 5. There is partial wave propagation through the large cluster, insufficient to create an oscillation

²Re-entrant VFO frequencies refer to the last 25 ms of the simulation, in order to get a pure re-entrant oscillation with no transitory externally driven waves.

Fig. 7 Parameter regimes for noise, re-entrant activity, and externally driven VFOs. The numerical score indicates the estimated probability of a behavior occurring within the first 50 ms: 1 stands for 100% probability of noise, 2 for 100% probability of re-entrant activity, and 3 for 100% probability of externally driven VFOs. Intermediate values stand for gradations in probability. For instance, 2.1 stands for a 90% probability of re-entrant activity and a 10% probability of externally driven VFOs



frequencies for externally driven VFOs ranged from 120 to 280 Hz, while the frequencies for re-entrant activity ranged from approximately 80 to 875 Hz. Thus re-entrant VFOs were a little faster on the average, but also had a much wider range of possible frequencies.

3.3 Mechanisms

Propagation failure at four-connected axons The results of the large network simulations suggest that the axonal plexus exhibits different behaviors depending on the amount of propagation failure in the network. There are a lot of propagation failures during noise, some during re-entrant activity, and none during externally driven VFOs. Propagation failure predominantly occurs at four-connected axons. For instance, in the example of noise shown in Fig. 6, 496 out of 498 propagation failures occurred at four-connected axons. In the example of re-entrant activity in Fig. 5, all seven propagation failures occurred at four-connected axons. There were no propagation failures in the externally driven VFOs in Fig. 4.

When studying examples of re-entrant activity in detail, we noticed that propagation failures occur when two waves arrive at a four-connected axon in quick succession. Sometimes a four-connected axon cannot

propagate the second wave while surrounding axons can. We therefore quantified propagation failure in simulations where two sequential waves propagate through a small network. Using the networks shown in Fig. 2, we stimulated axon 1 twice in a row and recorded when each axon fired. We then calculated t_f , the length of the time interval of propagation failure (see Fig. 3). The results of these simulations are summarized in Figs. 8 and 9, and reveal:

- The noise regime is the region in which four-connected axons cannot fire in response to a spike by only one neighbor.
- The re-entrant activity regime is the region in which four-connected axons can fire in response to a spike by a neighbor, but may fail to propagate two waves in quick succession.
- The externally driven VFO regime is the region in which four-connected axons propagate all waves reliably.

In Fig. 8, the black boundaries are those shown in Fig. 7. They border the region in which re-entrant activity occurs with probability $\geq 50\%$. The colored region where $0 < t_f < \infty$ shifts with the connectivity of the network. For instance, it shifts up a little if axon 3 has more neighbors and down a little if axon 3 has

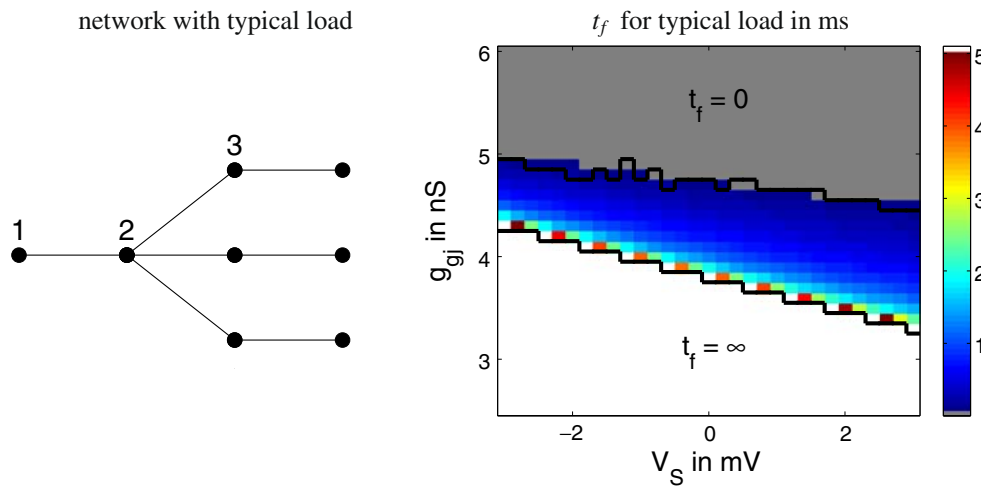


Fig. 8 Values of t_f for small network 4-2, in which neuron 2 has a typical gap-junctional load, reproduce the re-entrant activity regime with remarkably good accuracy. In the *grey region*, axon 2 fires whenever axon 1 fires. In the *white region*, axon 2 never fires in response to axon 1 firing. In the *colored region*, axon 2 fires

when axon 1 fires once, but does not necessarily fire again when axon 1 fires a second time. The length of time where propagation failure occurs (t_f) is given in ms in the *colored region*. (See Section 2 for details.) The *black boundaries* are the boundaries of the re-entrant activity regime shown in Fig. 7

fewer neighbors (data not shown). Thus the region in which re-entrant activity occurs is the region in which $0 < t_f < \infty$ for most four-connected axons. In Fig. 9, we show a similar analysis of the region in which re-

entrant activity is possible at all (that is, with probability > 0).

A similar analysis for three-connected axons, using axon 2 in small networks 3-1, 3-2, 3-3, and 3-4, confirms

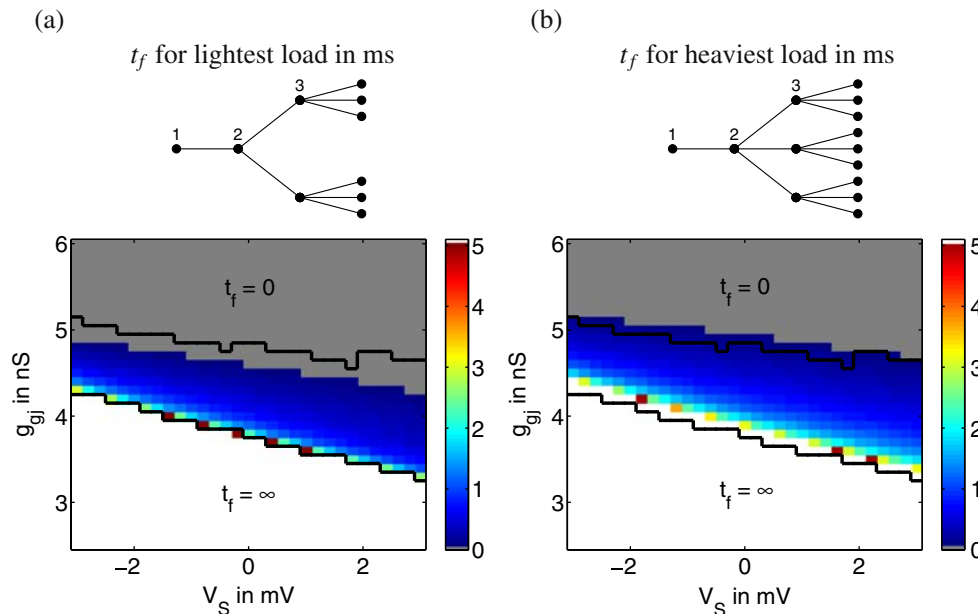


Fig. 9 Re-entry in the axonal plexus occurs only for those parameter values for which $0 < t_f < \infty$ for some four-connected axons. In this figure, the *black boundaries* enclose the area where re-entrant activity occurs at all, that is, with probability > 0 . (This is different from Fig. 8, where the black boundaries enclose the regime in which re-entry occurs with at least 50% probability.) Panel (a) shows that as V_s and g_{ij} increase, re-entrant activity

becomes possible as soon as signal propagation through the four-connected axons with the lightest gap-junctional load (axon 3 in the small network on the left) becomes possible. Panel (b) shows that as V_s and g_{ij} are raised further, re-entrant activity is no longer seen as soon as signal propagation through the four-connected axons with the heaviest gap-junctional load (axon 2 in the small network on the right) becomes reliable

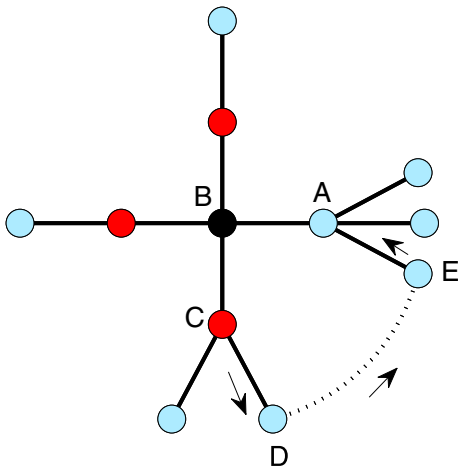


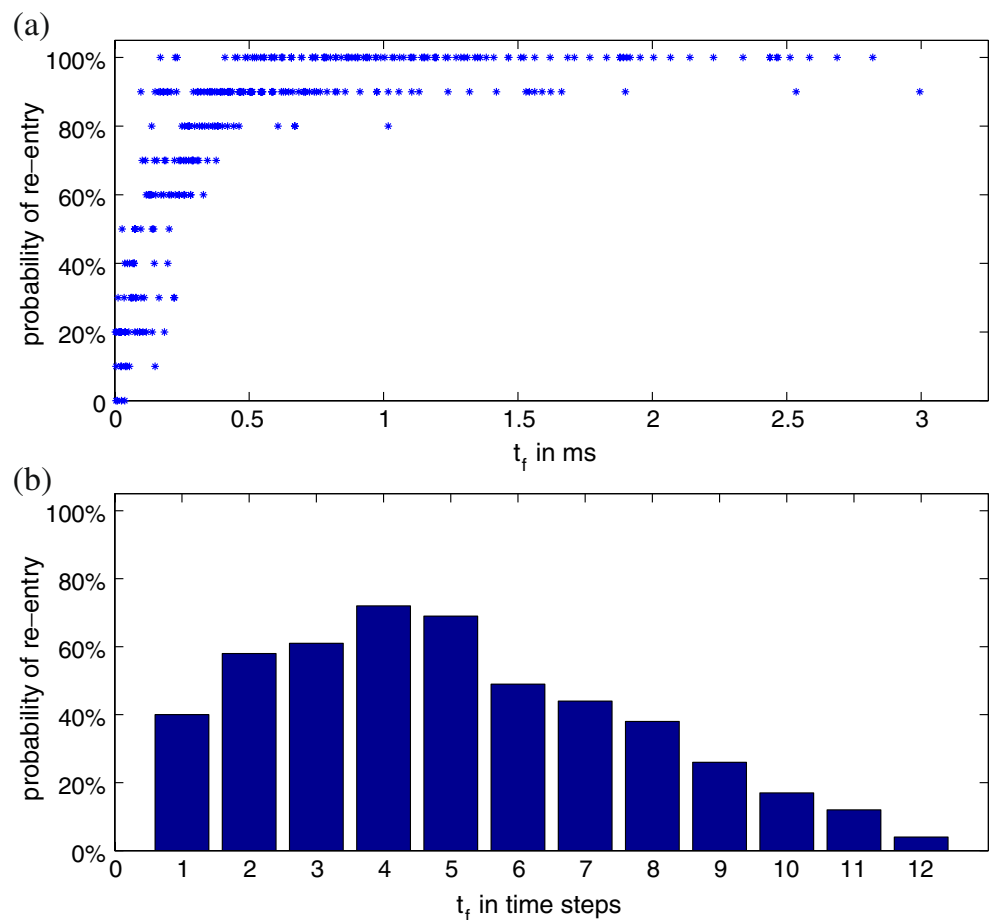
Fig. 10 A scenario where re-entry can occur due to propagation failure. Suppose that axon A fails to fire in response to B firing, causing an expanding wave to become asymmetric. The asymmetric wave then travels around a cycle connecting B to C . By the time the wave reaches A again, A is ready to fire and activity continues to propagate around the cycle

that three-connected axons propagate signals reliably in the re-entrant activity regime (the region bordered by solid lines in Figs. 7 and 8).

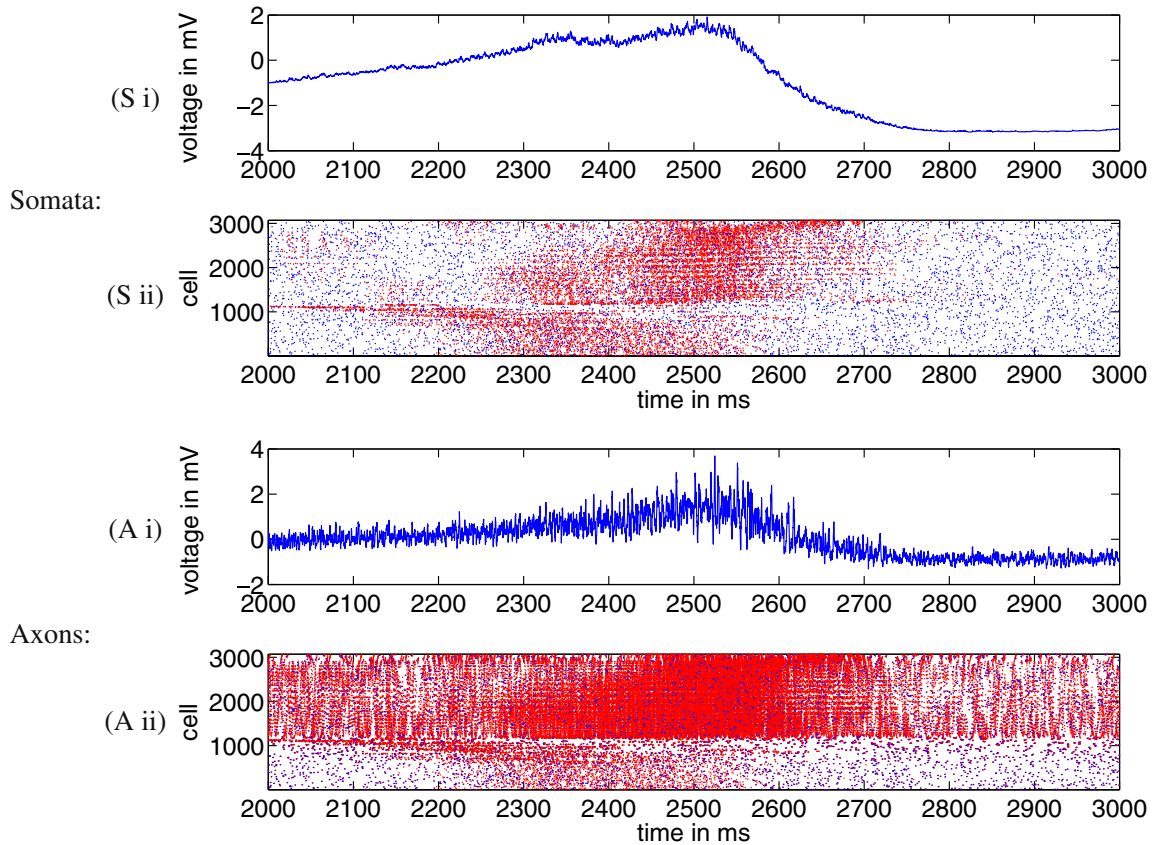
Four-connected axons segment the network We used the same large random network in all simulations of the axonal plexus used to create Fig. 7. In order to understand why four-connected axons determine the behavior of this entire network and to generalize our results to any random network, we analyzed 100 random networks with the network parameters described in Section 2. In any given network, only about 10% of the axons were four-connected. However, if all four-connected axons were disconnected from their neighbors, the network was split into many much smaller subclusters; there is no longer a large cluster on the order of the size of the network. Thus four-connected axons act as gateways between many small subclusters in the network.

Likelihood of cycles in the network When there is a propagation failure at a four-connected axon, how likely is it that activity will start propagating around a cycle? To analyze this, we first show an example of propagation failure leading to re-entry in Fig. 10; see the figure caption for the details. For the mechanism of Fig. 10, it is crucial that there be a cycle through A and

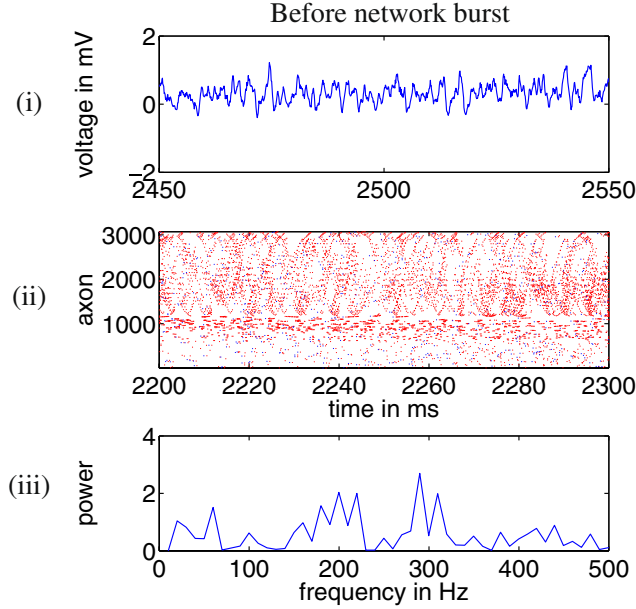
Fig. 11 Probability of re-entry during the first 50 ms as a “function” of t_f , the difference in refractory periods between four-connected and other cells: (a) axonal plexus, (b) altered CA (one time steps corresponds to 0.25 ms). In panel (a), t_f is computed from network 4-2 (see Fig. 8), and the probability of re-entry is taken from the computation underlying Fig. 7



(a)



(b)



(c)

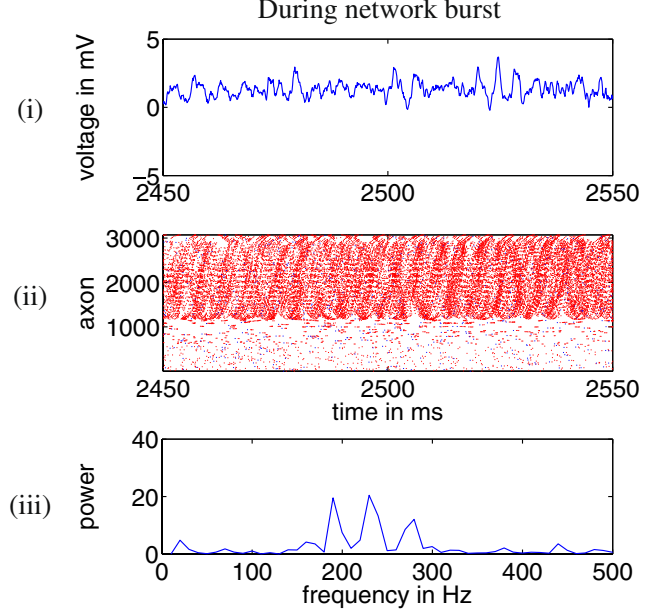


Fig. 12 A reproduction of the results shown in Traub et al. (1999, Figure 12). Panel (a) shows the average voltages of the somata (*S i*) and second-most-distal axonal compartments (*A i*) along with rastergrams of a network burst (*S ii*, *A ii*, red dots stand for spikes, blue dots stand for external stimulation). Panels (b) and (c) show activity between and during bursts in more

detail. Since the somatic voltage is less than 1 mV for most cells between bursts, the activity appears noisy. During a burst, most cells have a somatic voltage of at least 3 mV. Therefore, waves easily propagate through the large cluster. (Note that the vertical axes in the two bottom panels are scaled differently)

B. For a randomly selected four-connected axon, A , on the large cluster and a randomly selected neighbor, B , of A , we found that the probability of there being a cycle through A and B is quite high, about 2/3. Furthermore, when there is at least one cycle through A and B , there are usually several dozens of such cycles, with a minimum cycle length of about 10–20 axons (data not shown).

Frequency of re-entrant oscillations During re-entrant oscillations, all activity stems from a wave propagating around a cycle. The period of the oscillation is determined by the length L of this cycle, and by the time δ that it takes to propagate a spike from a given axon to a neighboring axon. We have found $\delta \approx 0.25$ ms in the range of values g_{gj} that yield re-entrant activity. With a minimum cycle length of 10–20 axons, this would yield a maximum frequency of 200–400 Hz for re-entrant oscillations, in good agreement with what is seen in the simulations.

Cellular automata confirm mechanisms

Mechanism of externally driven VFOs Lewis and Rinzel described a mechanism for externally driven VFOs in a CA in Lewis and Rinzel (2000). It is crucial for this mechanism that propagation from one axon to another never fails. Indeed we have shown that in the regime in which we see externally driven VFOs, propagation is reliable; see Figs. 7 and 9. We are confident that the mechanism of Lewis and Rinzel is in fact the one underlying externally driven VFOs in our simulations.

Mechanism of noise During noisy activity, four-connected axons cannot fire when a single neighbor fires. Our network analysis shows that four-connected axons partition the network into many much smaller subclusters. If four-connected axons *never* fire, then activity on each of these subclusters would be independent, and thus activity throughout the network would appear noisy. However, in the axonal plexus, even though four-connected axons cannot fire when only one neighbor fires, they can still fire when externally stimulated or when multiple neighbors fire simultaneously. We therefore altered the CA in Traub et al. (1999) so that four-connected axons were allowed to fire only when externally stimulated or when at least two neighbors fired simultaneously. We ran ten simulations of the altered CA; all of them exhibited noise, not oscillations. We therefore believe that during noisy activity, the failure to propagate signals through four-connected axons causes activity in different subclusters to be largely independent.

Mechanism of re-entrant activity Re-entry can only occur in the axonal plexus if expanding waves are not topologically closed, in the sense that the only way to cross from one side of a wave to the other in the network is to pass through the wave (Lewis and Rinzel 2000). Waves can break if there is propagation failure. Our simulations of small networks have shown that re-entrant activity is correlated to propagation failure in four-connected axons caused by heterogeneity in effective refractory periods. Our network analysis above indicates that propagation failure typically leads to activity traveling around a cycle in the network. To test this mechanism, we altered the CA in Traub et al. (1999) so that the four-connected cells have a longer refractory period than the other cells. The altered CA readily produces re-entrant activity. There is, however, a substantial difference in behavior between the altered CA and the axonal plexus: re-entrant activity is considerably more likely in the axonal plexus than in the altered CA, as shown in Fig. 11. See Discussion for a possible reason for this discrepancy.

3.4 Axonal plexus behavior with a full neuronal model

Our large network model was adapted from Traub et al. (1999). We now apply the results above to analyze the behavior of the full model of Traub et al. (1999), which includes somata and dendrites. The gap junction conductance in Traub et al. (1999) is 3.66 nS. In Fig. 12, we show our reproduction of the results of (Traub et al. 1999, Figure 12). The CA3 pyramidal cell model in Traub et al. (1999) bursts periodically. The somatic voltage falls to ~ -3 mV in between bursts. During bursts, the soma fires from a base voltage of ~ 3 mV. In Traub et al. (1999) and in our reproduction, all cells in the large cluster of the network burst roughly at the same time. Since $g_{gj} = 3.66$, four-connected cells only propagate waves when $V_s > 1$ mV (approximately) according to Fig. 7. Since $V_s < 1$ mV for every cell in between bursts, the axonal plexus exhibits noise. During bursts, $V_s > 1$ mV for most cells. Accordingly, waves propagate through the large cluster.

4 Discussion

Our model of an axonal plexus exhibits three distinct behaviors: noise, re-entrant activity, and externally driven VFOs. The somatic voltage and gap junction conductance determine the ability of four-connected axons to propagate waves, which in turn determines the behavior seen in the axonal plexus.

The key to understanding the dynamical behavior of the network is propagation failure. In our model, propagation failure is most likely to occur at highly connected nodes. The four-connected nodes play a special role because by construction of the network in Traub et al. (1999), they are the most highly connected. In different networks, nothing may be special about four-connected nodes. In general, we would expect that in many different model networks of electrically coupled cells, one will see target patterns when signal propagation is always reliable, spiral waves when propagation fails occasionally (this will typically happen in nodes with higher connectivity), and noise when propagation failures effectively break up the large cluster.

In Fig. 7, it appears that the transition from noise to spiral waves is abrupt, whereas the transition from spiral waves to target patterns is gradual. The transition from noise to spiral waves is in fact similar to the crossing of a percolation threshold: Below the threshold, there effectively is not a single large component of the network, whereas above it there is. The transition from spiral waves to target patterns is gradual, since it is a function of heterogeneity of effective refractory periods (see Fig. 11), which changes gradually as the gap junction conductance and somatic voltage are changed.

The frequencies of externally driven oscillations and those of re-entrant oscillations are often similar to each other (near 200 Hz). We believe that this is in fact largely accidental. The frequency of externally driven oscillations is primarily determined by the rate of the Poisson stimulation, and to some extent by the refractory period (Lewis and Rinzel 2000). As discussed in Section 3.3, the frequency of re-entrant activity depends on the cycle length and on the speed of propagation of action potentials from one cell to the next. Typical cycle lengths happen to be such that the frequency of re-entrant oscillations is often similar to that of externally driven oscillations, but (as stated at the end of Section 3.2) the range of observed frequencies is much greater for re-entrant oscillations.

Relation to other work This paper builds on the work of Traub et al. (1999) and Lewis and Rinzel (2000, 2001). Traub et al. (1999) introduced the original model. Lewis and Rinzel (2000) analyzed how expanding waves can form VFOs in a CA. In Lewis and Rinzel (2001), they showed that expanding waves can form VFOs in a more realistic model, using the axons of the model in Traub et al. (1999).

We changed the boundary condition on the axon initial segment from a sealed end (Lewis and Rinzel

2001) to a fixed somatic voltage V_s . In the more realistic model of Traub et al. (1999), V_s is not fixed, but typically changes more slowly than the voltage in the axons. The change in boundary condition makes the axons in our model less excitable than those in Lewis and Rinzel (2001). This brings us into the parameter regime in which re-entrant activity can be seen.

Figure 7 suggests that VFOs should be seen during the depolarization phase of slower oscillations. This is indeed the case; see for instance Grenier et al. (2001), Traub et al. (2003a). Figure 7 also suggests sharp transitions from noisy activity to VFOs and vice versa with changes of gap junction conductance or excitability; such a transition is seen in Traub and Bibbig (2000, Figure 5).

The work by Traub et al. shows that axonal plexus activity can drive gamma oscillations, including gamma oscillations without VFOs present (Traub et al. 2000, 2003b; Traub and Bibbig 2000). In the noise regime, there is partial wave propagation. This results in amplification of external stimulation and may suffice to drive gamma oscillations without the presence of VFOs; see for instance Traub et al. (2000, Figures 11, 12).

Our results are related to those of Ganser et al. (2007) and Tseng et al. (2008), which model small networks connected by gap junctions. In agreement with our findings, both papers demonstrate that re-entrant oscillations arise from asymmetric propagation block. Muratov et al. analyzed an abstract model of excitable media supporting both noise-driven target patterns and—depending on initial conditions—spiral waves (Muratov et al. 2007).

Maex and De Schutter studied another network of axons connected by gap junctions. In contrast with the network of Traub et al., their network is a regular, hexagonal grid (Maex and De Schutter 2007). Although Maex and De Schutter did not attribute the fast persistent oscillations observed in their model to activity traveling around closed loops, there are similarities between these oscillations and our re-entrant VFOs. Note in particular that the fast oscillations start spontaneously, and different waves look identical after the somata stop firing (Maex and De Schutter 2007, Figure 3B).

The fact that unidirectional propagation block due to heterogeneity of refractory periods can result in reentrant activity has been known in the literature on heart fibrillation for a very long time (Garrey 1924; Veenhuyzen et al. 2004). Atrial fibrillation has been studied by means of cellular automata at least since 1964 (Moe et al. 1964).

Gap junctions vs. IPSPs A number of authors have argued that VFOs may be generated not by axo-axonal gap junctions, but by synchronous firing of fast-spiking interneurons, with the local field potential reflecting inhibitory post-synaptic potentials (IPSPs) in pyramidal neurons (Engel et al. 2009; Kandel and Buzsáki 1997; Le Van Quyen et al. 2008; Ponomarkenko et al. 2004; Ylinen et al. 1995). Gap junctions among pyramidal axons are difficult to find experimentally, and interneurons can fire fast enough to maintain a VFO. On the other hand, there are experiments showing that VFOs (1) can persist under blockade of synaptic transmission, (2) are disrupted by gap junction blockers, and (3) are amplified by manipulations opening up gap junctions, in support of the hypothesis that VFOs originate from an axonal plexus (Draguhn et al. 1998; Grenier et al. 2001; Maier et al. 2003; Nimmrich et al. 2005; Roopun et al. 2010; Traub et al. 2003a, 2009). Also, while gap junctions among axons are rare, there is evidence for their existence by spikelets in pyramidal cells (Draguhn et al. 1998), dye coupling (Schmitz et al. 2001), and immuno-gold labeling (Hamzei-Sichani et al. 2007). There is a similar dichotomy for hypothesized mechanisms of VFOs in the cerebellum (de Solages et al. 2008; Middleton et al. 2008).

Limitations of the model Even though our results help explain aspects of the behavior of the model of Traub et al. (1999), there are still many questions that need to be addressed to fully explain the behavior seen in the original model, or in a real axonal plexus. Somata and dendrites complicate the system. They can provide feedback to the axonal plexus in multiple ways, for instance through spike reflection off the soma. As we see in our reproduction of Traub et al. (1999) (see Fig. 12), the fast oscillations may be less clean than in our simplified model. A spike in the soma can be considered a stimulus to the axon in the context of our model. It may therefore be difficult to test whether VFOs are re-entrant or not when somata and dendrites are present, unless the somata are not firing.

From Fig. 9, we know that heterogeneity in refractory periods is necessary for re-entrant activity. However, when we implemented heterogeneous refractory periods in the CA, the probability of re-entrant activity was much lower than in the axonal plexus. We note here an interesting difference between the dynamical properties of the axonal plexus and those of the CA which may account for this discrepancy.

In the axonal plexus, effective refractory periods can be direction-dependent. To see this, think of a wave passing through a four-connected axon in some direction, say from left to right. Suppose that a short

time later, a second wave arrives at the same four-connected axon. At this time, the axons to the left of the four-connected axon will be less hyperpolarized than the ones to the right, since the first wave passed from left to right. As a result, the second wave will be propagated more easily if it travels from right to left: The downstream axons (the ones on the left) are less hyperpolarized, and their shunting effect on the four-connected axon is therefore less strong. In our modified CA, the refractory periods are imposed based on connectivity, independent of activity patterns, and therefore direction-independent.

To see why direction-dependent effective refractory periods may promote re-entry, recall that re-entry typically occurs when a wave is blocked (by a four-connected axon) from traveling in one direction along a cycle, but permitted to travel in the other direction. There may be several four-connected axons along a cycle. Re-entry requires that a wave be blocked in one direction by one four-connected axon, but propagated past all four-connected axons along the cycle as it travels in the other direction. Direction-dependent effective propagation allows for this one-sided propagation more easily than a uniformly imposed longer refractory period for four-connected cells. For a much more detailed version of this argument, see (Munro 2008, Figure 4.52) and the discussion surrounding it.

Relevance of re-entrant activity to epilepsy Our findings suggest that re-entrant activity can readily occur in an axonal plexus. With somata present, the axonal plexus may shift from one regime to another, as in Fig. 12. Also, external drive may be intermittent in a more realistic context. Because re-entrant activity does not require external stimulation, re-entrant VFOs may persist longer than externally driven VFOs. Once re-entrant activity starts while the axonal plexus is in the re-entrant activity regime, it may continue even if the axonal plexus shifts to the externally driven VFO regime. The probability of re-entrant activity occurring depends on the time spent in the re-entrant activity regime. The slower the axonal plexus moves through the re-entrant activity regime, the more likely re-entrant activity will occur. This suggests a possible mechanism for seizure initiation: If the system lingers in the re-entrant regime, re-entrant activity becomes likely. Once it starts, it can persist and raise the level of excitation in the network.

The frequency of re-entrant VFOs depends crucially on the length of the re-entrant cycle generating the activity. There is a wide range of cycle lengths, and as a result a wide range of frequencies of re-entrant VFOs. Our model exhibits re-entrant VFOs with frequencies

up to 875 Hz, while the frequency of externally driven VFOs never exceeds 250 Hz. Our results suggest that fast ripples (> 250 Hz) often associated with epilepsy (Bragin et al. 1999, 2002, 2004; Staba et al. 2004; Urrestarazu 2007) may be re-entrant VFOs.

Summary An isolated axonal plexus can exhibit noise, re-entrant activity, or externally driven oscillations. Re-entrant activity can occur for a wide range of parameters. Re-entry typically occurs at moderate levels of excitation, but can generate longer-lasting activity than stimulus-driven VFOs. This, together with the fact that re-entrant VFOs can have much higher frequencies than externally driven VFOs, suggests that re-entrant activity may be involved in epilepsy.

Considerably more detail on many aspects of this work can be found in the first author's Ph.D. thesis (Munro 2008), on which this paper is based.

Acknowledgements We thank Roger Traub and Tim Lewis for valuable conversations and for making their codes available to us. We are also grateful to Stefanos Folias for many helpful discussions, and to Nancy Kopell for critiquing an earlier draft of this paper. We would also like to thank the reviewers, whose many comments helped improve this manuscript. This work was supported in part by National Science Foundation grant DMS0418832 (to CB).

Appendix: The power spectrum

In this appendix, we give, for completeness, the precise definition of “power spectrum” used in Section 2. In particular, we describe and motivate our choice of scaling here.

The discrete Fourier coefficients of a complex vector

$$v = (v_j)_{0 \leq j \leq N-1}$$

is the vector

$$(\hat{v}_k)_{k=\lceil -N/2 \rceil, \dots, \lceil N/2 - 1 \rceil}$$

($\lceil x \rceil$ denotes the smallest integer $\geq x$) with

$$\hat{v}_k = \frac{1}{N} \sum_{j=0}^{N-1} v_j e^{-2\pi i j k / N}.$$

The v_j can be reconstructed from the \hat{v}_k using the formula

$$v_j = \sum_{k=\lceil -N/2 \rceil}^{\lceil N/2 - 1 \rceil} \hat{v}_k e^{2\pi i j k / N}, \quad 0 \leq j \leq N-1.$$

Suppose that

$$v_j = w_j + X_j,$$

where the w_j are (deterministic) real numbers and the X_j are independent random variables with mean 0 and variance σ^2 . In this case, it is not hard to verify that

$$E(|\hat{v}_k|^2) = |\hat{w}_k|^2 + \frac{\sigma^2}{N}.$$

Thus the stochastic fluctuations add the power σ^2/N to each wave number.

The maximum power P referred to in Section 2 is defined as follows:

$$P = N \max \left\{ |\hat{v}_k|^2 : k = \left\lceil -\frac{N}{2} \right\rceil, \dots, \left\lceil \frac{N}{2} - 1 \right\rceil, k \neq 0 \right\}.$$

If v is dominated by a single Fourier mode (or a mixture of a small number of modes), P is large ($\sim N$). If v is dominated by noise, on the other hand, then P is only of moderate size ($\sim \sigma^2$).

References

- Bragin, A., Engel, J., Jr., Wilson, C. L., Fried, I., & Matherne, G. W. (1999). Hippocampal and entorhinal cortex high-frequency oscillations (100–500 Hz) in human epileptic brain and in kainic acid-treated rats with chronic seizures. *Epilepsia*, 40(2), 127–137.
- Bragin, A., Mody, I., Wilson, C. L., & Engel, J., Jr. (2002). Local generation of fast ripples in epileptic brain. *Journal of Neuroscience*, 22(5), 2012–2021.
- Bragin, A., Wilson, C. L., Almajano, J., Mody, I., & Engel, J., Jr. (2004). High-frequency oscillations after status epilepticus: Epileptogenesis and seizure genesis. *Epilepsia*, 45(9), 1017–1023.
- Clemens, Z., Mölle, M., Eross, L., Barsi, P., Halász, P., & Born, J. (2007). Temporal coupling of parahippocampal ripples, sleep spindles and slow oscillations in humans. *Brain*, 130(Pt. 11), 2868–2878.
- de Solages, C., Szapiro, G., Brunel, N., Hakim, V., Isope, P., Buisseret, P., et al. (2008). High-frequency organization and synchrony of activity in the Purkinje cell layer of the cerebellum. *Neuron*, 58(5), 775–788.
- Draguhn, A., Traub, R. D., Schmitz, D., & Jefferys, J. G. (1998). Electrical coupling underlies high-frequency oscillations in the hippocampus *in vitro*. *Nature*, 394(6689), 189–192.
- Engel, J., Jr., Bragin, A., Staba, R., & Mody, I. (2009). High-frequency oscillations: What is normal and what is not? *Epilepsia*, 50(4), 598–604.
- Erdős, P., & Rényi, A. (1960). On the evolution of random graphs. *Publications of the Mathematical Institute of the Hungarian Academy of Sciences*, 5, 17–61.
- Fisher, R. S., Webber, W. R., Lesser, R. P., Arroyo, S., & Uematsu, S. (1992). High-frequency EEG activity at the start of seizures. *Journal of Clinical Neurophysiology*, 9(3), 441–448.
- Gansert, J., Golowasch, J., & Nadim, F. (2007). Sustained rhythmic activity in gap-junctionally coupled networks of model neurons depends on the diameter of coupled dendrites. *Journal of Neurophysiology*, 98(6), 3450–3460.

- Garrey, W. E. (1924). Auricular fibrillation. *Physiological Reviews*, 4(2), 215–250.
- Greenberg, J. M., & Hastings, S. P. (1978). Spatial patterns for discrete models of diffusion in excitable media. *SIAM Journal on Applied Mathematics*, 34, 515–523.
- Grenier, F., Timofeev, I., & Steriade, M. (2001). Focal synchronization of ripples (80–200 Hz) in neocortex and their neuronal correlates. *Journal of Neurophysiology*, 86(4), 1884–1898.
- Grenier, F., Timofeev, I., & Steriade, M. (2003). Neocortical very fast oscillations (ripples, 80–200 Hz) during seizures: Intracellular correlates. *Journal of Neurophysiology*, 89(2), 841–852.
- Hamzei-Sichani, F., Kamasawa, N., Janssen, W. G., Yasumura, T., Davidson, K. G., Hof, P. R., et al. (2007). Gap junctions on hippocampal mossy fiber axons demonstrated by thin-section electron microscopy and freeze-fracture replica immunogold labeling. *Proceedings of the National Academy of Sciences of the United States of America*, 104(30), 12548–12553.
- Jacobs, J., LeVan, P., Chander, R., Hall, J., Dubeau, F., & Gotman, J. (2008). Interictal high-frequency oscillations (80–500 Hz) are an indicator of seizure onset areas independent of spikes in the human epileptic brain. *Epilepsia*, 49(11), 1893–1907.
- Kandel, A., & Buzsáki, G. (1997). Cellular-synaptic generation of sleep spindles, spike-and-wave discharges, and evoked thalamocortical responses in the neocortex of the rat. *Journal of Neuroscience*, 17(17), 6783–6797.
- Le Van Quyen, M., Bragin, A., Staba, R., Crépon, B., Wilson, C. L., & Engel, J., Jr. (2008). Cell type-specific firing during ripple oscillations in the hippocampal formation of humans. *Journal of Neuroscience*, 28(24), 6104–6110.
- Lewis, T. J., & Rinzel, J. (2000). Self-organized synchronous oscillations in a network of excitable cells coupled by gap junctions. *Network*, 11(4), 299–320.
- Lewis, T. J., & Rinzel, J. (2001). Topological target patterns and population oscillations in a network with random gap junctional coupling. *Neurocomputers*, 38–40, 763–768.
- Maex, R., & De Schutter, E. (2007). Mechanism of spontaneous and self-sustained oscillations in networks connected through axo-axonal gap junctions. *European Journal of Neuroscience*, 25(11), 3347–3358.
- Maier, N., Nimmrich, V., & Draguhn, A. (2003). Cellular and network mechanisms underlying spontaneous sharp wave-ripple complexes in mouse hippocampal slices. *Journal of Physiology*, 550(Pt. 3), 873–887.
- Middleton, S. J., Racca, C., Cunningham, M. O., Traub, R. D., Monyer, H., Knöpfel, T., et al. (2008). High-frequency network oscillations in cerebellar cortex. *Neuron*, 58(5), 763–774.
- Moe, G. K., Rheinboldt, W. C., & Abildskov, J. A. (1964). A computer model of atrial fibrillation. *American Heart Journal*, 67, 200–220.
- Munro, E. C. (2008). *The axonal plexus: A description of the behavior of a network of axons connected by gap junctions*. Ph.D. thesis, Tufts University.
- Muratov, C. B., Vanden-Eijnden, E., & Weinan, E. (2007). Noise can play an organizing role for the recurrent dynamics in excitable media. *Proceedings of the National Academy of Sciences of the United States of America*, 104(3), 702–707.
- Nimmrich, V., Maier, N., Schmitz, D., & Draguhn, A. (2005). Induced sharp wave-ripple complexes in the absence of synaptic inhibition in mouse hippocampal slices. *Journal of Physiology*, 563(Pt. 3), 663–670.
- Ponomarenko, A. A., Korotkova, T. M., Sergeeva, O. A., & Haas, H. L. (2004). Multiple GABA_A receptor subtypes regulate hippocampal ripple oscillations. *European Journal of Neuroscience*, 20(8), 2141–2148.
- Roopun, A. K., Simonotto, J. D., Pierce, M. L., Jenkins, A., Nicholson, C., Schofield, I. S., et al. (2010). A nonsynaptic mechanism underlying interictal discharges in human epileptic neocortex. *Proceedings of the National Academy of Sciences of the United States of America*, 107(1), 338–343.
- Schmitz, D., Schuchmann, S., Fisahn, A., Draguhn, A., Buhl, E. H., Petrasch-Parwez, E., et al. (2001). Axo-axonal coupling: A novel mechanism for ultrafast neuronal communication. *Neuron*, 31(5), 831–840.
- Staba, R. J., Wilson, C. L., Bragin, A., Jhung, D., Fried, I., & Engel, J., Jr. (2004). High-frequency oscillations recorded in human medial temporal lobe during sleep. *Annals of Neurology*, 56(1), 108–115.
- Traub, R. D., Schmitz, D., Jefferys, J. G., & Draguhn, A. (1999). High-frequency population oscillations are predicted to occur in hippocampal pyramidal neural networks interconnected by axo-axonal gap junctions. *Neuroscience*, 92(2), 407–426.
- Traub, R. D., Bibbig, A., Fisahn, A., LeBeau, F. E., Whittington, M. A., & Buhl, E. H. (2000). A model of gamma-frequency network oscillations induced in the rat CA3 region by carbachol *in vitro*. *European Journal of Neuroscience*, 12(11), 4093–4106.
- Traub, R. D., & Bibbig, A. (2000). A model of high-frequency ripples in the hippocampus based on synaptic coupling plus axon–axon gap junctions between pyramidal neurons. *Journal of Neuroscience*, 20(6), 2086–2093.
- Traub, R. D., Whittington, M. A., Buhl, E. H., LeBeau, F. E., Bibbig, A., Boyd, S., et al. (2001). A possible role for gap junctions in generation of very fast EEG oscillations preceding the onset of, and perhaps initiating, seizures. *Epilepsia*, 42(2), 153–170.
- Traub, R. D. (2003). Fast oscillations and epilepsy. *Epilepsy Currents*, 3(3), 77–79.
- Traub, R. D., Cunningham, M. O., Gloveli, T., LeBeau, F. E., Bibbig, A., Buhl, E. H., et al. (2003a). GABA-enhanced collective behavior in neuronal axons underlies persistent gamma frequency oscillations. *Proceedings of the National Academy of Sciences of the United States of America*, 100(19), 11047–11052.
- Traub, R. D., Pais, I., Bibbig, A., LeBeau, F. E., Buhl, E. H., Hormuzdi, S. G., et al. (2003b). Contrasting roles of axonal (pyramidal cell) and dendritic (interneuron) electrical coupling in the generation of neuronal network oscillations. *Proceedings of the National Academy of Sciences of the United States of America*, 100(3), 1370–1374.
- Traub, R. D., Contreras, D., & Whittington, M. A. (2005). Combined experimental/simulation studies of cellular and network mechanisms of epileptogenesis *in vitro* and *in vivo*. *Journal of Clinical Neurophysiology*, 22(5), 330–342.
- Traub, R. D., Middleton, S. J., Knöpfel, T., & Whittington, M. A. (2008). Model of very fast (> 75 Hz) network oscillations generated by electrical coupling between the proximal axons of cerebellar Purkinje cells. *European Journal of Neuroscience*, 28(8), 1603–1661.
- Traub, R. D., Duncan, R., Russell, A. J., Baldeweg, T., Tu, Y., Cunningham, M. O., et al. (2009). Spatiotemporal patterns of electrocorticographic very fast oscillations (>80 Hz) consistent with a network model based on electrical coupling between principal neurons. *Epilepsia*, published online December 2009.

- Tseng, S. H., Tsai, L. Y., & Yeh, R. R. (2008). Induction of high-frequency oscillations in a junction-coupled network. *Journal of Neuroscience*, 28(28), 7165–7173.
- Urrestarazu, E., Chander, R., Dubeau, F., & Gotman, J. (2008). Interictal high-frequency oscillations (100–500 Hz) in the intracerebral EEG of epileptic patients. *Brain*, 130(Pt. 9), 2354–2366.
- Veenhuyzen, G. D., Simpson, C. S., & Abdollah, H. (2004). Atrial fibrillation. *CMAJ*, 171(7), 755–760.
- Worrell, G. A., Parish, L., Cranstoun, S. D., Jonas, R., Baltuch, G., & Litt, B. (2004). High-frequency oscillations and seizure generation in neocortical epilepsy. *Brain*, 127(Pt. 7), 1496–1506.
- Ylinen, A., Bragin, A., Nádasdy, Z., Jandó, G., Szabó, I., Sik, A., et al. (1995). Sharp wave-associated high-frequency oscillation (200 Hz) in the intact hippocampus: Network and intracellular mechanisms. *Journal of Neuroscience*, 15(1 Pt. 1), 30–46.